THE ASTROPHYSICAL JOURNAL, 496:210–215, 1998 March 20

AN *ASCA* OBSERVATION OF M51 (NGC 5194): IRON K EMISSION FROM AN OBSCURED ACTIVE GALACTIC NUCLEUS

Y. TERASHIMA,[1] A. PTAK,[2,3] R. FUJIMOTO,[4] M. ITOH,[5] H. KUNIEDA,[1] K. MAKISHIMA,[6] AND P. J. SERLEMITSOS[2]
Received 1997 June 30; accepted 1997 October 24

ABSTRACT

We present an *ASCA* observation of the nearby spiral galaxy M51 (NGC 5194). We detected hard X-ray emission with a photon index of ~ 1.4 and a luminosity of $L_X \sim 1.1 \times 10^{40}$ ergs s^{-1} in the 2–10 keV band (assuming a distance of 9.6 Mpc). A strong fluorescent iron K line (equivalent width ~ 900 eV) was detected at 6.4 keV in the X-ray spectra. Such an intense iron line is characteristic of Seyfert 2 galaxies and strongly suggests the presence of a heavily obscured active galactic nucleus (AGN). However, the X-ray image is extended even at energies above 2 keV. From the strong iron line and the extended hard X-ray image we speculate that the AGN is obscured by matter with a hydrogen column density more than several times 10^{23} cm^{-2} and that the observed 2–10 keV X-ray flux is not dominated by emission from the AGN but rather by other components, such as low-mass X-ray binaries, which typically dominate the X-ray emission of normal spiral galaxies. Emission lines from O K, Ne K, Fe L, Mg K and Si K were detected in the soft energy spectra, which indicate the presence of hot gas. The soft component is well represented by a Raymond-Smith thermal plasma model (with $kT \sim 0.4$ keV), which suggests a lower iron abundance (<0.1 solar) than other elements (~ 0.1–0.4 solar), or by a two temperature ($kT \sim 0.3$ keV and $kT \sim 0.8$ keV) model with ~ 0.1 solar abundance, which is reminiscent of the X-ray–emitting gas in starburst galaxies.

Subject headings: galaxies: individual (M51) — galaxies: nuclei — X-rays: galaxies

1. INTRODUCTION

The nearby spiral galaxy M51 (NGC 5194) is known as the "Whirlpool galaxy" and has been intensively studied at various wavelengths. On the basis of optical emission-line studies, the M51 nucleus has been classified as a Seyfert 2 or a low-ionization nuclear emission-line region (LINER) (Stauffer 1982; Filippenko & Sargent 1985; Ho, Filippenko, & Sargent 1997). Therefore, the presence of a low-luminosity active galactic nucleus (AGN) has previously been inferred.

One of the most convincing pieces of evidences for an AGN is the detection of a hard X-ray point source at the nucleus. The *Einstein* HRI detected X-ray emission from M51 with a luminosity $L_X = 3.0 \times 10^{40}$ ergs s^{-1} in the 0.2–4.0 keV band (we assume a distance of 9.6 Mpc throughout this paper; Sandage & Tammann 1975). However, the HRI image of the nucleus is clearly extended and provides only an upper limit ($L_{0.2-4.0\,\mathrm{keV}} < 1.5 \times 10^{39}$ ergs s^{-1}) for the luminosity of a point source at the nucleus (Palumbo et al. 1985). A *ROSAT* HRI observation confirmed that the X-ray source at the nucleus is extended (Ehle, Pietsch, & Beck 1995). The *ROSAT* PSPC spectrum of the M51 nucleus is fitted with a $kT \sim 0.4$ keV thermal plasma model (Marston et al. 1995; Read, Ponman, & Strickland 1997). Such a soft X-ray spectrum also supports the idea that the AGN does not dominate the nuclear soft X-ray emission. The *ROSAT* PSPC and HRI also detected eight point sources with X-ray luminosities around 10^{39} ergs s^{-1} in M51 superposed on diffuse X-ray emission. A *Ginga* observation detected hard X-ray emission with a photon index $\Gamma = 1.4$ and an X-ray luminosity in the 2–20 keV bandpass of $(1.2 \pm 0.6) \times 10^{41}$ ergs s^{-1} from a ~ 1 deg^2 field containing M51 (Makishima et al. 1990). The *Ginga* spectrum can also be fitted with a $kT = 7$ keV thermal bremsstrahlung model plus a power law ($\Gamma = 1.6$) absorbed with $N_H \sim 4 \times 10^{23}$ cm^{-2}. Makishima et al. (1990) proposed a scenario to explain both the *Einstein* and *Ginga* data in which the AGN is obscured and only the harder portion of the spectrum is dominated by X-rays from an active nucleus. The visual and UV-band images taken by the *Hubble Space Telescope* show X-shaped dust lanes (Maran & Kinney 1993; Maoz et al. 1996). A dense molecular disk with $N_H > 3.0 \times 10^{23}$ cm^{-2} around the nucleus is also revealed by HCN ($J = 1 \rightarrow 0$) and CO ($J = 1 \rightarrow 0$) observations (Kohno et al. 1996). Some of this material may account for the X-ray–absorbing material.

The presence of an obscured nucleus can be tested directly by imaging spectroscopic observations in hard X-rays above 2 keV. *ASCA* (Tanaka, Inoue, & Holt 1994) enables us to obtain X-ray images and spectra up to 10 keV with high sensitivity. This capability is quite useful in searching for evidence of low-luminosity AGNs as shown by the detection of hard point sources in galaxies (Serlemitsos, Ptak, & Yaqoob 1996), such as M106 (NGC 4258, Makishima et al. 1994), M81 (NGC 3031, Ishisaki et al. 1996), M104 (NGC 4594, Terashima et al. 1994), and NGC 1097 (Iyomoto et al. 1996). Detection of the iron K lines provides still more convincing evidence (e.g., Iyomoto et al. 1997; Ptak et al. 1996).

In addition to searching for an AGN, the study of thermal emission from hot gas in spiral galaxies is also an important aspect of observing spiral galaxies (Makishima 1994). The *ROSAT* PSPC observations revealed extended emission in some nearby spiral galaxies (Read et al. 1997

[1] Department of Physics, Nagoya University, Chikusa-ku, Nagoya 464-01, Japan.
[2] Laboratory for High Energy Astrophysics, NASA/GSFC, Greenbelt, MD 20771.
[3] University of Maryland, College Park, MD 20742.
[4] Institute of Space and Astronautical Science, 3-1-1 Yoshinodai, Sagamihara, Kanagawa 229, Japan.
[5] Faculty of Human Development, Kobe University, Nada-ku, Kobe 657, Japan.
[6] Department of Physics, University of Tokyo, Bunkyo-ku, Tokyo 113, Japan.

and references therein), including M51 (Ehle et al. 1995). *ASCA* spectra of NGC 4258 indicate emission lines from various species that are probably of thermal origin (Makishima et al. 1994). *ASCA* measurements of the mass and elemental abundances of the hot gas present in spiral galaxies is critical to our understanding of the origin of this gas.

We observed M51 with *ASCA* and obtained X-ray images and spectra in the 0.4–10 keV energy band. We present the observational results and discuss the origin of the X-ray emission.

2. OBSERVATIONS AND DATA REDUCTION

M51 (NGC 5194) was observed by *ASCA* (Tanaka et al. 1994) on 1993 May 11 during the performance-verification (PV) phase. *ASCA* has two solid-state imaging spectrometers (SIS, hereafter SIS0 and SIS1; Burke et al. 1991) and two gas imaging spectrometers (GIS, hereafter GIS2 and GIS3; Ohashi et al. 1996; Makishima et al. 1996) as focal-plane detectors of four identical X-ray telescopes (XRTs; Serlemitsos et al. 1995), which enable us to obtain X-ray images at energies up to 10 keV with a spatial resolution of 3′ half-power diameter (HPD). The SIS has superior energy resolution ($\Delta E/E = 2\%$ at 5.9 keV), while the GIS has higher efficiency in the hard X-ray band. The SIS has better spatial resolution than the GIS, since the sharp core of the XRT point-spread function is somewhat smeared by a position determination error of the GIS ($\sim 0'.5$). The SIS sensors were operated in 4 CCD faint/bright mode. The faint and bright mode data from two SIS sensors were added together after appropriate gain corrections. The GIS sensors were operated in pulse-height normal mode, and the spread discriminator was not enabled at the time of this observation. Data from the two GIS sensors were also added together. We used the nominal data selection criteria: times were excluded when the elevation angle from the Earth rim was less than 5°, the geomagnetic cutoff rigidity was less than 6 GeV c^{-1}, and the telescope was in the South Atlantic Anomaly. Additionally, the condition that the elevation angle from the day-Earth rim was greater than 25° was also applied to the SIS data. We obtained a net integration time of 36 ks for the SIS and 39 ks for the GIS after data screening.

The SIS and GIS spectra were extracted from a region within 3′ of the M51 nucleus in radius and fitted simultaneously. Only data from SIS0 chip1 and SIS1 chip3 were used for extracting SIS spectra, since most of the source flux fell on these chips. Background data were accumulated from a source-free region of the same field. The spectra were binned so that each spectral bin contained at least 20 counts in order to use χ^2 fitting. The count rates of M51 for the SIS and GIS were 0.05 counts s^{-1} and 0.03 counts s^{-1}, respectively. Although the companion galaxy NGC 5195 is located $\sim 4'$ to the north of M51, its X-ray flux is about one-quarter that of M51 in the 0.5–10 keV band, according to the present *ASCA* observation. Therefore, the flux from NGC 5195 does not significantly affect the results on M51.

3. RESULTS

3.1. *X-Ray Images*

The *ASCA* SIS0 + SIS1 image of M51 in the 0.5–10 keV band is shown in Figure 1. The X-ray emission from M51 and the companion NGC 5195 is clearly detected. The discrete sources detected in the *ROSAT* (Marston et al. 1995; Ehle et al. 1995; Read et al. 1997) and *Einstein* (Palumbo et al. 1985) observations are not clearly seen in the *ASCA* image, and only hints of the sources A and B in Palumbo et al. (1985) are seen.

In order to evaluate the spatial extent of the X-ray emission, we examined a brightness profile of the SIS0 image (the SIS have superior spatial resolution to the GIS). We used a rectangular region parallel to the detector x-axis, as shown in Figure 1. The brightness profile projected onto the detector x-axis in this region is shown in Figure 2 for the 0.5–2 keV, 2–5 keV, and 5–10 keV energy bands. The histogram in Figure 2 represents the point-spread function (PSF) of the *ASCA* XRT + SIS in each energy range at the source position projected onto the detector x-axis in the same way as actual data. The brightness distribution is thus clearly extended in the 0.5–2 keV and 2–5 keV energy bands as compared to the PSF. On the other hand, the image in the 5–10 keV band is consistent with the PSF, although photon statistics are poor.

3.2. *X-Ray Spectra*

The SIS and GIS spectra are shown in Figure 3. These spectra clearly show emission lines around 1 keV, which indicate the presence of sub-keV, optically thin plasmas, and neither the simple power law nor the thermal bremsstrahlung models provide acceptable fits. A single-temperature Raymond-Smith thermal plasma model (Raymond & Smith 1977) also fitted the data poorly, and significant hard tail residuals remained. Additionally, emission line–like residuals were also seen around 6.4 keV. Accordingly, we fitted the spectra with a combination of a Raymond-Smith plasma, a power law, and a Gaussian model, where we assumed Galactic absorption ($N_{\rm H} = 1.3 \times 10^{20}$ cm^{-2}; Stark et al. 1992). The fitting results are summarized in Table 1. The reduced χ^2 was 1.242 for 142 dof in this model. However, emission line–like residuals still remained at ~ 0.65 keV, 0.9–1.0 keV, and ~ 1.9 keV, which we identified as H-like O K, He and H-like Ne K, and He-like Si K emission lines, respectively. These residuals suggest a nonsolar abundance ratio and/or a multi-temperature plasma. We further examined two models: (1) power-law + $2kT$ Raymond-Smith plasma + Gaussian model and (2) power-law + variable abundance Raymond-Smith plasma + Gaussian model. The best-fit parameters are also summarized in Table 1. We obtained significant improvement in the fit, and the reduced χ^2 was 1.01 and 0.997 for 140 and 138 degrees of freedom (dof), using models (1) and (2), respectively. Then we allowed the absorption column density for the hard component to vary in models (1) and (2), where the hydrogen column density for the Raymond-Smith component was fixed to the Galactic value. We obtained only an upper limit of $N_{\rm H} = 1.2 \times 10^{22}$ cm^{-2} at 90% confidence for one interesting parameter ($\Delta\chi^2 = 2.7$).

The SIS and GIS spectra and the best-fit model for the variable abundance case are shown in Figure 2. The X-ray luminosities of the hard power-law component and the Raymond-Smith component are 1.1×10^{40} ergs s^{-1} in the 2–10 keV bandpass and 1.2×10^{40} ergs s^{-1} in the 0.5–2 keV bandpass, respectively. The X-ray luminosity of the power-law component is about 6 times lower than that obtained with *Ginga* (6.7×10^{40} ergs s^{-1}) in the 2–10 keV band, while the spectral slope of the hard component ($\Gamma = 1.43^{+0.17}_{-0.38}$) agrees well with the *Ginga* results of a power-law

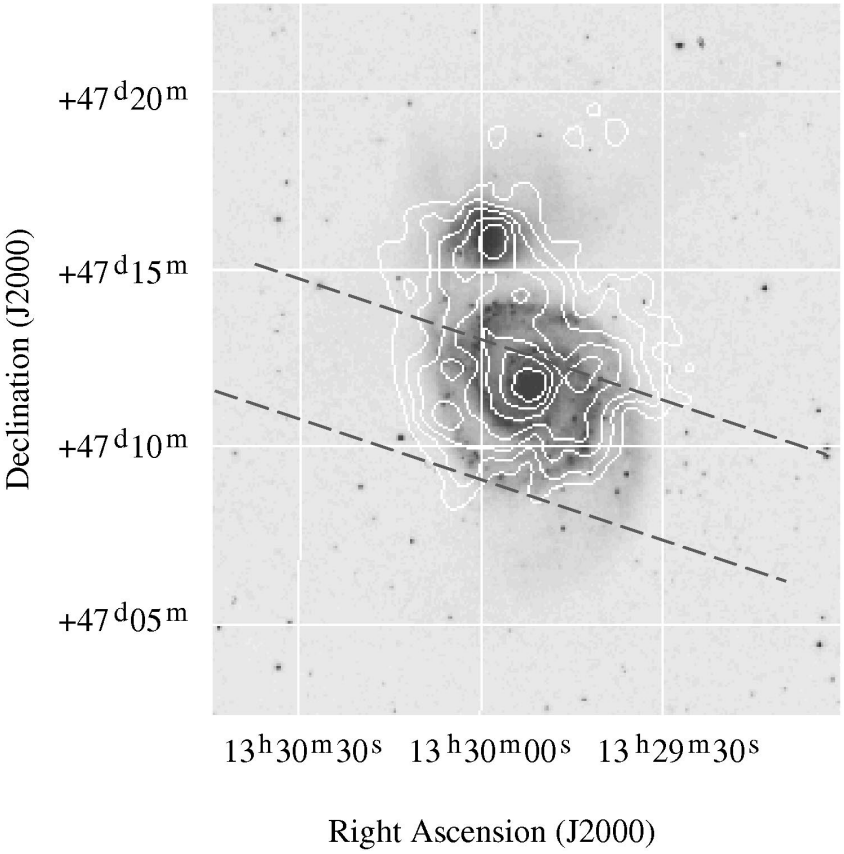

FIG. 1.—Contour map of M51 and NGC 5195 taken with SIS detectors (SIS0 + SIS1) superposed on optical image. Background is not subtracted. The contour levels are logarithmically spaced. The region between dashed lines is used to make a projected brightness profile presented in Fig. 2.

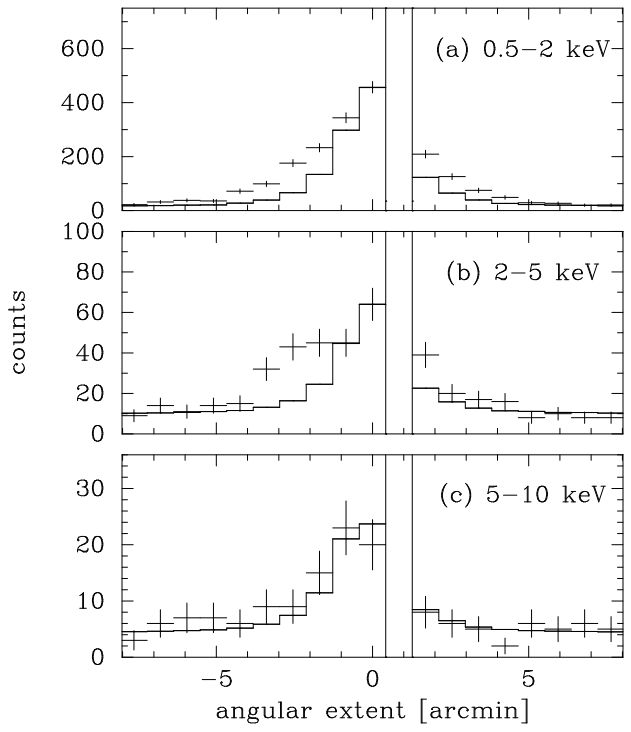

FIG. 2.—Brightness profile projected onto the detector x-axis in (*a*) 0.5–2 keV, (*b*) 2–5 keV, and (*c*) 5–10 keV. The crosses are SIS0 data, and the histogram represents the PSFs of XRT + SIS added on the background level. The region at an angle of $\sim 1'$ corresponds to the interchip gap of the SIS detector.

fit in the 2–20 keV band ($\Gamma = 1.43 \pm 0.08$). In this model the addition of the narrow Gaussian line at 6.4 keV improved χ^2 by $\Delta\chi^2 = 15.7$ for the two additional parameters. Therefore, the line feature is statistically significant at more than the 99.9% confidence level for 2 additional degrees of freedom (line-center energy and line intensity). The line-

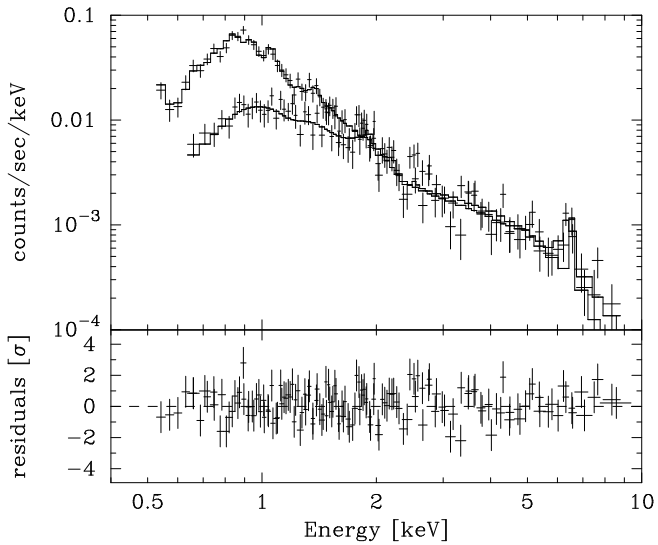

FIG. 3.—*ASCA* SIS and GIS spectra of M51. The solid lines represent the best-fit model of a combination of a variable-abundance Raymond-Smith model, a power law, and a Gaussian.

TABLE 1

RESULTS OF MODEL FITTING TO THE SIS AND GIS SPECTRA OF M51

Parameter	Power Law + RS	Power Law + $2kT$ RS	Power Law + Variable Abundance RS
N_H (10^{20} cm^{-2})	1.3 (fixed)	1.3 (fixed)	1.3 (fixed)
Hard Component:			
Power-law Photon Index Γ	1.13 (0.84–1.35)	1.01 (0.94–1.34)	1.43 (1.05–1.60)
Line energy (keV)	6.41 (6.26–6.49)	6.41 (6.26–6.49)	6.40 (6.28–6.48)
Equivalent width (eV)	720 (390–1120)	720 (410–1090)	910 (530–1320)
Soft component:			
kT (keV)	0.50 (0.46–0.55)	0.29 (0.26–0.32)	0.42 (0.38–0.52)
	...	0.82 (0.78–0.86)	...
Abundance:			
(Solar)	0.027 (0.020–0.035)	0.10 (0.086–0.12)	...
O	...	...	0.11 (0.054–0.20)
Ne	...	...	0.29 (0.27–0.49)
Mg	...	...	0.12 (0.012–0.30)
Si	...	...	0.42 (0.18–0.81)
Fe	...	...	0.055 (0.033–0.065)
χ^2/dof	176.4/142	141.0/140	137.6/138

NOTE.—Quoted errors in parentheses are at the 90% confidence level for one interesting parameter.

center energy, $6.40^{+0.08}_{-0.12}$ keV, implies the K line of nearly neutral iron. The equivalent width was determined to be 910^{+410}_{-380} eV for the variable abundance case. The confidence contours for the line-center energy and the line flux are shown in Figure 4.

4. DISCUSSION

4.1. *Hard X-Ray Emission and an Iron Emission Line*

The X-ray spectrum from M51 is represented by a combination of a hard component with a photon index of ~ 1.4 and a thermal emission component with $kT \sim 0.4$ keV. The luminosity of the hard component is $L_{2-10\,\mathrm{keV}} = 1.1 \times 10^{40}$ ergs s^{-1}. This luminosity is about 6 times lower than that measured with *Ginga* (Makishima et al. 1990). Additionally a strong fluorescent iron emission line is found at 6.4 keV with an equivalent width of ~ 900 eV.

In normal spiral galaxies, X-ray emission is dominated by discrete sources such as low-mass X-ray binaries (LMXBs) (Fabbiano 1989; Makishima et al. 1989). The X-ray luminosity of M51 obtained with *ASCA* is only a factor of 2 larger than that of the normal spiral galaxy M31, which is dominated by LMXBs (Makishima et al. 1989). The X-ray

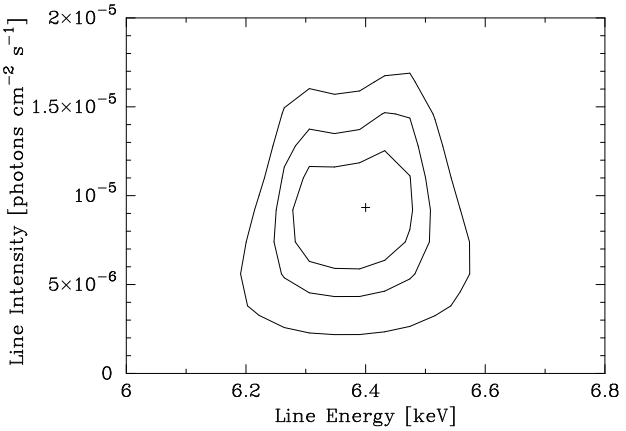

FIG. 4.—Confidence contours for the iron line energy and normalization. Contour levels correspond to 68%, 90%, and 99% confidence levels from inside to outside.

to B-band luminosity ratio of M51, $L_{2-10\,\mathrm{keV}}/L_B \sim 5.9 \times 10^{-5}$, is also close to those of normal spiral galaxies (e.g., $L_X/L_B = 3.5 \times 10^{-5}$ for M31; Makishima et al. 1989). Therefore a significant portion of the observed hard X-ray luminosity from M51 is likely to come from the superposition of LMXBs. The extended image in the 2–5 keV band also supports this interpretation. However, the observed spectral slope of the hard component ($\Gamma \sim 1.4$) is harder than those of LMXBs, which are roughly equivalent to $\Gamma \sim 1.8$. Moreover, the observed strong iron emission line cannot be explained by the emission from LMXBs. Therefore, the presence of an additional flat spectral component, accompanied by an iron line, is strongly inferred.

The iron emission line at 6.4 keV is of fluorescence origin from cold material irradiated by a strong X-ray source (an Fe line produced thermally from hot gas would have had an energy in excess of 6.7 keV). The large equivalent width of ~ 900 eV is expected primarily when the X-ray source is obscured by hydrogen column density significantly greater than 10^{23} cm^{-2} (Makishima 1986). Thus the observed iron emission line strongly suggests the presence of an obscured X-ray source. A strong iron line of an equivalent width as large as ~ 1 keV, which is not accompanied by high absorption of low-energy X-rays, has been seen in heavily obscured Seyfert 2 galaxies, in which the hydrogen column density is thought to exceed 10^{24} cm^{-2} (e.g., NGC 1068, Koyama et al. 1989; NGC 4945, Iwasawa et al. 1993; NGC 1365, Iyomoto et al. 1997). Their continua are interpreted as being dominated by X-rays scattered into the line of sight by partially ionized material in the opening part of the obscuring torus.

In M51, however, the X-ray image above 2 keV is extended by more than several arcminutes in diameter, which requires that scattering material is extended over galaxy scales. A possibility for reconciling the spectral results with the extended image in the 2–5 keV band is that the AGN emission contributes only to the hardest end of the *ASCA* spectra. We examined a spectral model consisting of a combination of a soft thermal component, a LMXB component approximated by a 7 keV thermal bremsstrahlung model (Makishima et al. 1989), and an absorbed power law from an AGN. Since the photon statistics are limited,

we fixed the photon index for the power-law component at 1.4, which is typical for Seyfert 2 galaxies observed with *Ginga* (Awaki et al. 1991), and the temperature of the thermal bremsstrahlung component at 7 keV. We assumed the hydrogen column density at the Galactic value for the soft thermal component and the LMXB component. For the power-law component, the hydrogen column density was fixed to values between 5×10^{23} cm^{-2} and 1×10^{24} cm^{-2}. A good fit was obtained for these assumed values of absorption column densities with a reduced χ^2 of 0.985 (138 dof) for $N_{\rm H} = 5 \times 10^{23}$ cm^{-2}, for example. The intrinsic luminosity of the absorbed component, corrected for absorption, varied from 1.5×10^{40} to 3.7×10^{40} ergs s^{-1} when the absorption column was changed from 5×10^{23} cm^{-2} to 1×10^{24} cm^{-2}. The equivalent width of the iron line was then calculated as $\sim 1.1 \pm 0.6$ keV. An equivalent width that exceeds 1 keV is rather large to be a typical obscured Seyfert 2 galaxy (e.g., Awaki et al. 1991), although the errors are large. This large equivalent width may also be a result of variability of the continuum emission from the nucleus. If the light crossing time over the distance from the nucleus to the emitting region of the iron line is larger than the variability timescale of the nucleus, a variation of iron line flux would be delayed, relative to a continuum variation. Therefore, in this case, after the continuum emission decreases, a large iron line equivalent width might be expected.

Alternatively, it is also possible that reflected X-rays from an AGN dominate the hard band spectrum. In such a case, a large equivalent width of the iron K line up to 1–2 keV with respect to the reflected continuum would be expected (George & Fabian 1991). Indeed, an extremely strong iron line is observed from the Seyfert 2 nucleus in NGC 6552 (Fukazawa et al. 1994; Reynolds et al. 1994) and the Circinus galaxy (Matt et al. 1996). The observed equivalent width of the iron line is ~ 0.9 keV and ~ 2 keV in NGC 6552 and the Circinus galaxy, respectively. These remarkable X-ray spectra are interpreted as being dominated by X-rays reflected from cold matter. A spectral model for the hard component, consisting of thermal bremsstrahlung (fixed to $kT = 7$ keV) and a reflected continuum (the *plrefl* model in XSPEC), also reproduced the observed spectrum (with a reduced χ^2 of 0.997 for 138 dof; Fig. 5). For the reflection component, we assumed an incident photon index of 2.0 and a face-on disk that subtends a solid angle 2π, as seen from the irradiating source. An equivalent width of $1.5^{+0.9}_{-0.7}$ keV was obtained with respect to the reflected continuum. The 2–10 keV luminosity of the reflected component was 3.9×10^{39} ergs s^{-1}, while that of the bremsstrahlung component was 7.7×10^{39} ergs s^{-1}. The best-fit parameters for the soft Raymond-Smith component are similar to the results presented in Table 1. These results are consistent with the reflection-dominated model, which can explain the extended image in the 2–5 keV band, the compact image in the 5–10 keV band, and the large equivalent width of the iron emission line, at the same time.

The 2–10 keV luminosity we measured is about 6 times lower than that derived with *Ginga* (Makishima et al. 1990). Although we cannot rule out the possibility that the *Ginga* LAC field of view was contaminated by other sources, the overall spectral slope ($\Gamma \sim 1.4$) obtained with *Ginga* in the 2–20 keV band is very similar to that derived with *ASCA*. Therefore, the apparent flux discrepancy between *Ginga* and *ASCA* may be due to time variations in the AGN of M51. In fact, when we increase the incident luminosity of the reflection component in Figure 5 by ~ 5 times and raise its escape fraction up to $\sim 10\%$, the spectrum and flux obtained with the *Ginga* LAC can be approximately reproduced. A gradual luminosity change of this order has actually been observed from the M81 nucleus (Ishisaki et al. 1996).

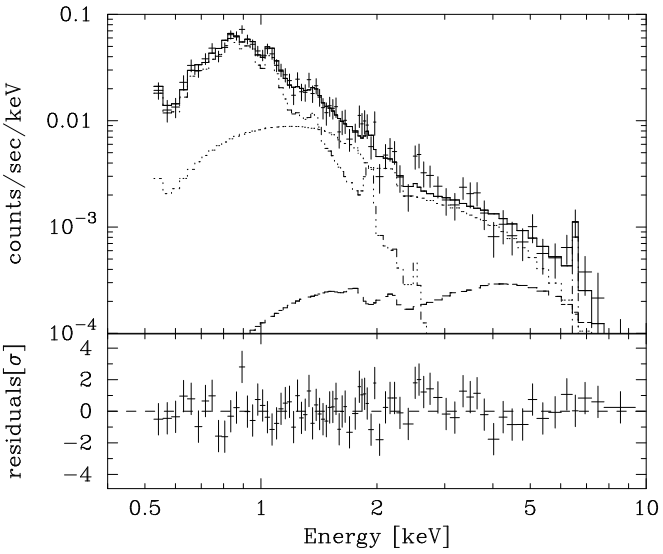

FIG. 5.—Reflection plus LMXB model fit for the hard component. Although fitting of SIS and GIS data were done simultaneously, only SIS data are shown for clarity.

4.2. *Thermal Emission*

The presence of diffuse hot gas across the galaxy has been pointed out on the extended X-ray images of M51 obtained with *ROSAT* (Ehle et al. 1995; Marston et al. 1995; Read et al. 1997). The *ASCA* spectra, exhibiting various low-energy emission lines (O VIII, Ne IX, Ne X, Mg XI, Fe L line complex), give strong support to the *ROSAT* results.

The results of a variable-abundance Raymond-Smith plasma plus a hard-component model fit indicates $kT \sim 0.4$ keV and a low iron abundance compared to other elements such as O, Ne, Mg, and Si. The 2 kT Raymond-Smith plus a hard component model also gives an acceptable fit. Hot gas components with these characteristics have been observed from starburst galaxies such as M82 and NGC 253 (Ptak et al. 1997; Moran & Lehnert 1997; Tsuru et al. 1997). Furthermore, the ratio of X-ray luminosity to far-infrared luminosity M51, $\log (L_{\rm X}/L_{\rm FIR}) = -4.1$, is similar to those of starburst galaxies (Heckman, Armus, & Miley 1990; David, Jones, & Forman 1992), where $L_{\rm X}$ is the luminosity of the Raymond-Smith component and $L_{\rm FIR}$ is the far infrared luminosity of 60 μm plus 100 μm *IRAS* measurements calculated using equation (1) in David et al. (1992). These facts suggest that the X-ray–emitting gas originates mainly from active star formation. Thus, our results support the starburst-driven winds interpretation of the diffuse emission in the *ROSAT* images (Read et al. 1997; Ehle et al. 1995), especially from a spectral point of view.

5. CONCLUSION

We observed the nearby spiral galaxy M51 with *ASCA* and detected a soft thermal emission and a hard X-ray emission of photon index ~ 1.4. A strong fluorescence iron emission line of equivalent width 900 eV is also detected. This

iron line strongly suggests the presence of a obscured active nucleus. The X-ray image in the 5–10 keV band is consistent with a point source, and this also supports the presence of an AGN. On the other hand, since X-ray images in the 2–5 keV band are extended, X-rays from an AGN do not dominate the X-ray flux in the 2–5 keV band and an AGN should be obscured below 5 keV. The extended X-rays in the 2–5 keV band are probably dominated by discrete sources such as LMXBs. The *ASCA* spectra is well represented by a combination of a soft thermal, plasma, LMXBs, and an obscured AGN emission by hydrogen column density more than 5×10^{23} cm^{-2} or a reflected continuum from an AGN. This model explains the X-ray image, the continuum shape, and an iron emission line at the same time. The soft thermal component is represented by either $kT \sim 0.4$ keV plasma with low iron abundance or 2 kT plasmas, which is consistent with a starburst-driven winds origin.

The authors express their gratitude to all the *ASCA* team members. Y. T. thanks the Japan Society for the Promotion of Science for the support of young scientists in the form of fellowships.

REFERENCES

Awaki, H., Koyama, K., Inoue, H., & Halpern, J. P. 1991, PASJ, 43, 195
Burke, B. E., Mountain, R. W., Harrison, D. C., Bautz, M. W., Doty, J. P., Ricker, G. R., & Daniels, P. J., 1991, IEEE Trans. ED-38, 1069
David, L. P., Jones, C., & Forman, W. 1992, ApJ, 388, 82
Ehle, M., Pietsch, W., & Beck, R. 1995, A&A, 295, 289
Fabbiano, R. 1989, ARA&A, 27, 87
Filippenko, A. V., & Sargent, W. L. W. 1985, ApJS, 57, 503
Fukazawa, Y., et al. 1994, PASJ, 46, L141
George, I. M., & Fabian, A. C. 1991, MNRAS, 249, 352
Heckman, T. M., Armus, L., & Miley, G. K. 1990, ApJS, 74, 833
Ho, L. C., Filippenko, A. V., & Sargent, W. L. W. 1997, ApJS, 112, 315
Ishisaki, Y., et al. 1996, PASJ, 48, 237
Iwasawa, K., et al. 1993, ApJ, 409, 155
Iyomoto, N., Makishima, K., Fukazawa, Y., Tashiro, M., & Ishisaki, Y. 1997, PASJ, 49, 425
Iyomoto, N., Makishima, K., Fukazawa, Y., Tashiro, M., Ishisaki, Y., Nakai, N., & Taniguchi, Y. 1996, PASJ, 48, 231
Kohno, K. Kawabe, R., Tosaki, T., & Okumura, S. K. 1996, ApJ, 461, L29
Koyama, K., Inoue, H., Tanaka, Y., Awaki, H., Takano, S., Ohashi, T., & Matsuoka, M. 1989, PASJ, 41, 731
Makishima, K. 1986, in The Physics of Accretion onto Compact Objects; ed. K. O. Mason et al. (Berlin: Springer)
———. 1994, in New Horizon of X-Ray Astronomy, ed. F. Makino & T. Ohashi (Tokyo: Universal Acad. Press), 171
Makishima, K., et al. 1989, PASJ, 41, 697
———. 1994, PASJ, 46, L77
———. 1996, PASJ, 48, 171
Makishima, K., Ohashi, T., Kondo, H., Palumbo, G.G.C., & Trinchieri, G. 1990, ApJ, 365, 159
Maoz, D., Filippenko, A. V., Ho, L. C., Macchetto, F. D., Rix, H-W., & Schneider, D. P. 1996, ApJS, 107, 215
Maran, S. P., & Kinney, A. L. 1993, PASP, 105, 447
Marston, A. P., Elmegreen, D., Elmegreen, B., Forman, W., Jones, C., & Flanagan, K. 1995, ApJ, 438, 663
Matt, G., et al. 1996, MNRAS, 281, L69
Moran, E. C., & Lehnert, M. D. 1997, ApJ, 478, 172
Ohashi, T., et al. 1996, PASJ, 48, 157
Palumbo, G. G. C., Fabbiano, G., Fransson, C., & Trinchieri, G. 1985, ApJ, 298, 259
Ptak, A., Yaqoob, T., Serlemitsos, P., Kunieda, H., & Terashima, Y. 1996, ApJ, 459, 542
Ptak, A., Serlemitsos, P., Yaqoob, T., Mushotzky, F., & Tsuru, T. 1997, AJ, 113, 1286
Raymond, J. C., & Smith, B. W. 1977, ApJS, 35, 419
Reynolds, C. S., Fabian, A. C., Makishima, K., Fukazawa, Y., & Tamura, T. 1994, MNRAS, 268, L55
Read, A. M., Ponman, T. J., & Strickland, D. K. 1997, MNRAS, 286, 626
Sandage, A., & Tammann, G. A. 1975, ApJ, 196, 313
Serlemitsos, P. J., et al. 1995, PASJ, 47, 105
Serlemitsos, P. J., Ptak, A., & Yaqoob, T. 1996, in The Physics of LINERs in View of Recent Observations, ed. M. Eracleous et al. (San Francisco: ASP), 70
Stark, A. A., Gammie, C. F., Wilson, R. W., Bally, J., Linke, R. A., Heiles, C., & Hurwitz, M. 1992, ApJS, 79, 77
Stauffer, J. R. 1982, ApJ, 262, 66
Tanaka, Y., Inoue, H., & Holt, S. S. 1994, PASJ, 46, L37
Terashima, Y., Serlemitsos, P. J., Kunieda, H., & Iwasawa, K. 1994, in New Horizon of X-Ray Astronomy, ed. F. Makino & T. Ohashi (Tokyo: Universal Acad. Press), 523
Tsuru, T., et al. 1997, PASJ, submitted